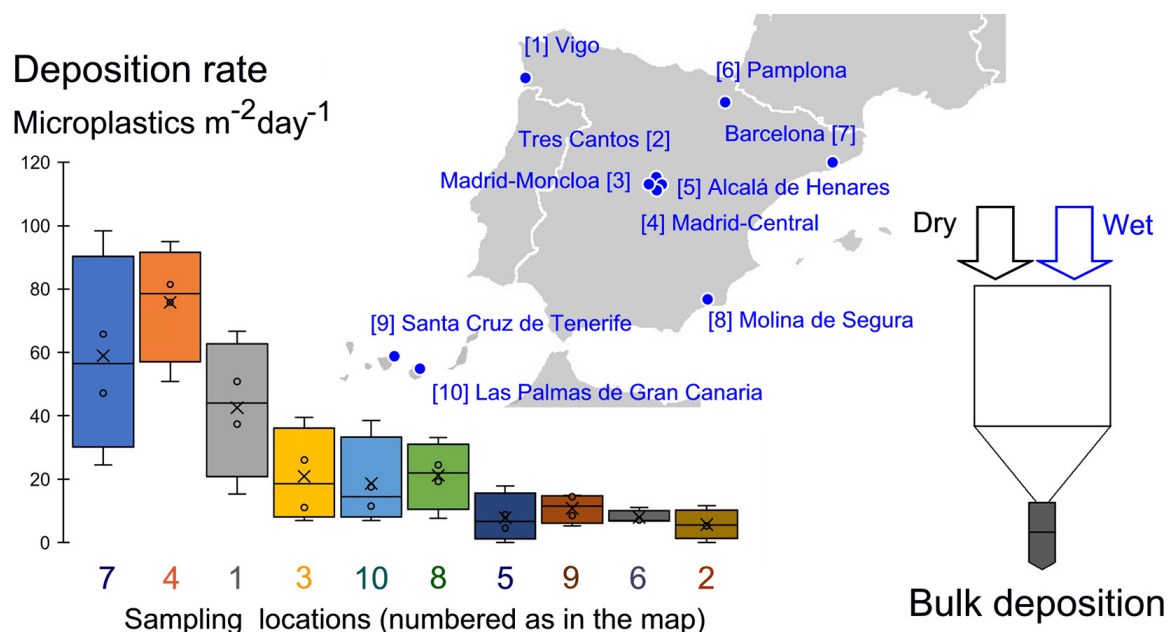


A nationwide monitoring of atmospheric microplastic deposition

*This manuscript version is made available in fulfillment of publisher's policy.
Please, cite as follows:*

Carlos Edo, Francisca Fernández-Piñas, Francisco Leganes, May Gómez, Ico Martínez, Alicia Herrera, Cintia Hernández-Sánchez, Javier González-Sálamo, Javier Hernández Borges, Joaquín López-Castellanos, Javier Bayo, Cristina Romera-Castillo, David Elustondo, Carolina Santamaría, Rocío Alonso, Héctor García-Gómez, Rosario Gonzalez-Cascon, Virtudes Martínez-Hernández, Junkal Landaburu-Aguirre, Mónica Incera, Jesús Gago, Beatriz Noya, Ricardo Beiras, Soledad Muniategui-Lorenzo, Roberto Rosal, Miguel González-Pleiter. A nationwide monitoring of atmospheric microplastic deposition. *Science of The Total Environment* 905, 166923, 2023.

<https://doi.org/10.1016/j.scitotenv.2023.166923>



A nationwide monitoring of atmospheric microplastic deposition

Carlos Edo¹, Francisca Fernández-Piñas^{2,3}, Francisco Leganes^{2,3}, May Gómez⁴, Ico Martínez⁴, Alicia Herrera⁴, Cintia Hernández-Sánchez⁵, Javier González-Sálamo⁵, Javier Hernández-Borges⁵, Joaquín López-Castellanos⁶, Javier Bayo⁶, Cristina Romera-Castillo⁷, David Elustondo⁸, Carolina Santamaría⁸, Rocío Alonso⁹, Héctor García-Gómez⁹, Rosario Gonzalez-Cascon¹⁰, Virtudes Martínez-Hernández¹¹, Junkal Landaburu-Aguirre¹¹, Mónica Incera¹², Jesús Gago¹², Beatriz Noya¹³, Ricardo Beiras¹³, Soledad Muniategui-Lorenzo¹⁴, Roberto Rosal^{1,*}, Miguel González-Pleiter^{2,3*}

¹Department of Chemical Engineering, Universidad de Alcalá, E-28871 Alcalá de Henares, Madrid, Spain

²Department of Biology, Faculty of Science, Universidad Autónoma de Madrid, E-28049 Madrid, Spain

³Centro de Investigación en Biodiversidad y Cambio Global (CIBC-UAM), Universidad Autónoma de Madrid, Madrid, Spain

⁴Ecophysiology of Marine Organisms (EOMAR), IU-ECOAQUA, Universidad de Las Palmas de Gran Canaria, Spain

⁵Applied Analytical Chemistry Research Group (AChem), Universidad de La Laguna, San Cristóbal de La Laguna, Spain

⁶Department of Chemical and Environmental Engineering, Technical University of Cartagena, Spain

⁷Instituto de Ciencias del Mar-CSIC, Barcelona, Spain

⁸Instituto de Biodiversidad y Medioambiente (BIOMA), Universidad de Navarra, Pamplona, Spain

⁹Centro de Investigaciones Energéticas, Medioambientales y Tecnológicas (CIEMAT), Madrid, Spain

¹⁰Department of Environment, National Institute for Agriculture and Food Research and Technology (INIA), Madrid, Spain

¹¹IMDEA-Water Institute, Alcalá de Henares, Madrid, Spain

¹²1 Instituto Español de Oceanografía (IEO-CSIC), Centro Oceanográfico de Vigo, Spain

¹³Centro de Investigación Marina de la Universidad de Vigo (CIM-UVigo), Spain

¹⁴University of Coruña, Grupo Química Analítica Aplicada (QANAP), Coruña, Spain

Abstract

Plastic production continues to increase every year, yet it is widely acknowledged that a significant portion of this material ends up in ecosystems as microplastics (MPs). Among all the environmental compartments affected by MPs, the atmosphere remains the least well-known. Here, we conducted a one-year simultaneous monitoring of atmospheric MPs deposition in ten urban areas, each with different population sizes, economic activities, and climates. The objective was to assess the role of the atmosphere in the fate of MPs by conducting a nationwide quantification of atmospheric MP deposition. To achieve this, we deployed collectors in ten different urban areas across continental Spain and the Canary Islands. We implemented a systematic sampling methodology with rigorous quality control/quality assurance, along with particle-oriented identification and quantification of anthropogenic particle deposition, which included MPs and industrially processed natural fibres. Among the sampled MPs, polyester fibres were the most abundant, followed by acrylic polymers, polypropylene, and alkyd resins. Their equivalent sizes ranged from 22 µm to 398 µm, with a median value of 71 µm. The particle size distribution of MPs showed fewer large particles than expected from a three-dimensional fractal fragmentation pattern, which was attributed to the higher mobility of small particles, especially fibres. The atmospheric deposition rate of MPs ranged from 5.6 to 78.6 MP m^{-2} day $^{-1}$, with the higher values observed in densely populated areas such as Barcelona and Madrid. Additionally, we detected natural polymers, mostly cellulosic fibres with evidence of industrial processing, with a deposition rate ranging from 6.4 to 58.6 particles m^{-2} day $^{-1}$. There was a positive correlation was found between the population of the study area and the median of atmospheric MP deposition, supporting the hypothesis that urban areas act as sources of atmospheric MPs. Our study presents a systematic methodology for monitoring atmospheric MP deposition.

1. Introduction

Plastic pollution has become a significant global concern, with plastic production steadily increasing and reaching nearly 400 million tons in 2021 (Plastics Europe, 2022). Plastic debris are termed as microplastics (MP), plastic particles smaller than 5 mm in their

larger dimension. MPs can be directly manufactured in this size as components of personal care products such as toothpaste or exfoliating creams, among other uses. These are referred to as primary MPs. Conversely, secondary MPs are produced during the fragmentation of larger plastic items under the effect of physicochemical and biological factors.

MPs have been detected in all environmental compartments, even in remote and polar areas (Evangelou et al., 2020; González-Pleiter et al., 2021; Pastorino et al., 2021). However, their presence in the atmosphere has only recently come to light. Urban

*Corresponding authors: roberto.rosal@uah.es, mig.gonzalez@uam.es, Available online: September 12, 2023

areas appear to be pivotal in the generation of various types of MPs (dos Santos Galvão et al., 2022). Polyester fibres dominate the composition of atmospheric fibres, likely due to their mechanical characteristics and widespread use in textiles (Batool et al., 2022). Tire and road wear particles also represent another significant source of plastic pollution in cities, but their understanding remains limited due to challenges in identifying small particles that contain synthetic rubber with a substantial proportion (40–60 %) of additives (Sun et al., 2022). The proximity to emission sources may explain the high deposition rates observed in large cities like London ($771 \text{ MPs m}^{-2} \text{ day}^{-1}$) or Hamburg ($275 \text{ MPs m}^{-2} \text{ day}^{-1}$).

The atmospheric compartment is also a relevant transport pathway, allowing the long-range dispersal of small plastic particles (González-Pleiter et al., 2021). The mobility of MPs in the atmosphere seems to be favoured by their low density and depends on their size and shape. For instance, the presence of small MPs in snow recovered from a glacier in the Tibetan Plateau was attributed to long-range transport from heavily polluted areas in the Indo-Gangetic Plain. This study revealed relatively high deposition rates ranging $20.9\text{--}26.2 \text{ MPs m}^{-2} \text{ day}^{-1}$, indicating that MPs would end up in rivers and downstream ecosystems (Wang et al., 2020). Additionally, it has been estimated that the annual emission of MPs from Asia and adjacent oceans reaches 370 Gg, the smallest particles being transported $>1000 \text{ km}$ away from their source. Several studies demonstrated that MPs are removed from the atmosphere during rain episodes, similar to other particulate matter. Improper treatment of stormwater, due to the overload of wastewater treatment plants, could emerge as a significant pathway for the entry of MPs into the aquatic environment (Österlund et al., 2023).

The goal of this work was to perform a nationwide assessment of atmospheric MPs deposition to shed light on the role of the atmosphere in the fate of plastic pollution. To achieve this, we deployed a set of collectors in ten urban areas with varying population sizes, economic activities, and climatic specificities. The sampling was conducted over four one-month periods distributed across four consecutive years' seasons. Special attention was given to establishing a unified methodology for sampling, identifying, and quantifying atmospheric MP deposition.

2. Materials and methods

2.1. Study area and sampling procedure

Deposition samples were simultaneously collected from 10 different locations across continental Spain and the Canary Islands during the spring (May-2021), summer (July-2021), autumn (November-2021) and winter (January-2022). The sampling sites included the cities of Vigo, Pamplona, Barcelona, Molina de Segura, Madrid (two sampling points), Tres Cantos, and Alcalá de Henares in continental Spain and in Santa Cruz de Tenerife (Tenerife Island) and Las Palmas de Gran Canaria (Gran Canaria Island) in the Canary Islands archipelago (Fig. 1). These locations were selected based on their diverse population sizes, economic activities, and climates. The main characteristics of these locations can be found in Tables S1 and S2 of the Supplementary Material (SM).

The sampling involved deploying a set of custom-made metal collectors (Fig. S1, SM) for one month and four times throughout each consecutive seasons of a meteorological year. The collectors were designed to capture bulk deposition, which included both dry deposition and fallout after rainwater events. The collectors were funnel-shaped and entirely made of stainless steel with an opening of 11 cm diameter and 20 cm height from the top to a receiving cone (according to Guide to Meteorological Instruments and Methods of Observation of World Meteorological Organization) that fitted to laboratory standard Pyrex™ borosilicate glass bottles (ISO 4796-1:2016) (Fig. S1, SM). A glass bottle with a capacity of at least 1 L was connected to the collector. Therefore, all components of the collectors were plastic-free.

At each site and period, two collectors were deployed to assess the intrinsic variability of the sampling method. Throughout the entire sampling period at each site, the accumulated precipitation was recorded using Hellmann-type pluviometers placed nearby. The capacity of the bottles used for the collectors was adjusted according to the expected precipitation. In case the accumulated precipitation exceeded the capacity of the receiving bottle, a procedure was established to substitute the bottle with a new empty one, following the same disassembly procedure described below for end of the prescribed exposure time. This event happened only once. To prevent vandalism, all collectors were positioned in protected areas, such as the enclosure of the National Institute for Agriculture and Food Research and Technology, shown in Fig. S1 (Supplementary Materials). The collectors were placed at a height between 1.7 and 2.6 m above the ground, following the guidelines of the Norwegian Institute of Air Research (Innovation NILU, 2020). During the assembly and disassembly



Figure 1: Sampling locations for MPs deposition.

stages at the beginning and end of the collection period, an extra collector was employed as a procedural control (see Section 2.4).

Once the collection was completed, after 30 or 31 days of continuous sampling, collectors were covered with aluminium foil and transported to the laboratory. The collectors including their procedural controls, and irrespective of the amount of rain recovered, were carefully washed with 150 mL of with ultrapure water (Milli-Q water, 0.22 µm Millipak filter) to remove any material that may have adhered to the walls. The collected samples were then filtered through 25 µm stainless steel filters. Subsequently, the filters were transferred to glass Petri dish. The Petri dishes containing filters from the samples were preserved at 4 °C whenever possible to prevent the growth of microorganisms and sent to the laboratory located at the University of Alcalá (Madrid) for processing.

2.2. Identification and quantification of microplastics

The filters were placed in 33 % H₂O₂ at 60 °C for 24 h to remove organic matter. Afterwards, the samples could be handled without any flotation and separation step. Potentially anthropogenic particles, which included all putative non-natural particles, were identified, photographed, and measured using a stereomicroscope. Length and width of the particles were measured with ImageJ software. In this study, the term 'particle' was used to refer to plastics as well as artificial non-plastic particles (ANPP) and natural particles. Following GESAMP guidelines, the particles were further classified into different morphological classes, namely fibres, fragments, and films (GESAMP, 2019). Fragments included a minor set of

beads or spheres. Particles with an aspect ratio equal to or >3:1 (as traditionally established for man-made mineral fibres) were considered fibres. If not, they were classified as fragments unless one dimension was at least one tenth lower than the other two, in which case they were categorized as films.

Polymer identification was conducted with micro-Fourier-transformed infrared spectroscopy (micro-FTIR) using a Perkin-Elmer Spotlight 200i micro-FTIR apparatus equipped with an MCT detector and operated in transmission mode on KBr discs with spectral resolution 8 cm⁻¹ and a wavelength in the 550–4000 cm⁻¹ range. Due to the high number of particles with probable anthropogenic origin found, a subsample sufficiently large to ensure an error <5 % was analysed with infrared spectroscopy as explained below. The spectra were compared with built-in databases or reference spectra specifically created using aged plastics. Pearson correlation >65 % was considered enough for positive identification according to other studies (González-Pleiter et al., 2021; Liu et al., 2019).

2.3. Modelling and statistics

All positively identified MPs were individually characterized based on their two orthogonal projected dimensions, d₁ and d₂, namely length and width for fragments and films and length and diameter for fibres. For close to isometric particles, it has been demonstrated that d_v, the diameter of the sphere with the same volume as the particle, can be approximated using projected images by the following expression (Rosal, 2021):

$$d_v \simeq \sqrt[3]{(d_1 d_2) \frac{(d_1 + d_2)}{2}} \quad (1)$$

For the case of films, the third, smallest and non-

recorded dimension, was assumed to be one tenth of the smallest among the other two. For fibres, dv was computed assuming cylindrical shape. The mass of individual particles was estimated using the tabulated average density for each polymer.

The abundance of plastic particles usually follows a power law with size for particles exceeding a certain critical size that depends on the type of sample (Kooi and Koelmans, 2019). The underlying cause is that break-up of a single particle generates a significant number of smaller fragments. The relationship can be mathematically represented as a probability density function denoted as $p(x)$ in which x represents size and α is the scaling parameter of the power law:

$$p(x) = p(x \leq X \leq x + dx) \propto x^{-\alpha} \quad (2)$$

If $\alpha > 1$, the cumulative frequency distribution function (CFD) that gives the probability of finding a particle with higher or equal than x , $P(X \geq x)$ can be easily derived:

$$P(x) = p(X \geq x) = \left(\frac{x}{x_{min}} \right)^{-\alpha+1} \quad (3)$$

The preceding equation, which represents the normalized integral of Eq. (2), holds true when $\alpha > 1$, and is applicable for sizes higher than a reference lower limit, x_{min} . The scaling parameter depends on the dimension of the fractal fragmentation process that generates the distribution and on the probability of fragmentation (fragility) of the material (Turcotte, 1986; Wang et al., 2020). Computing the exponent of the power law distribution requires the use of maximum likelihood estimation to avoid large errors in the fitting of experimental data due to the logarithmic scale. The method maximizes the likelihood of having observed a set of data x_1, x_2, \dots, x_n under a certain statistical model. The uncertainty in parameter estimation can be obtained using a bootstrapping procedure that consists of generating multiple data sets from which the exponent of the power law and the estimation for x_{min} are recalculated. Details on the bootstrapping procedure can be found elsewhere (Gillespie, 2015). To assess the correlation of plastic deposition rate with explanatory variables, one-way ANOVA (p -value < 0.05) was used. Throughout this work, all values are presented as mean \pm standard error.

2.4. Quality assurance/quality control assessment

The possible contamination of samples with external materials was avoided by using the following procedure. Before sampling, aluminium foil packets with aluminium foil inside were heated in an oven

at over 300 °C for 4 h to remove all possible plastic contamination. Collectors, glass materials, tweezers and needles were cleaned with ultrapure water three times, covered with aluminium foil, and heated in an oven at over 300 °C for 4 h to remove all possible plastic contamination. Stainless steel 25 µm filters were placed in clean glass Petri dishes, wrapped with aluminium foil, and heated in an oven at over 300 °C for 4 h to remove all possible plastic contamination. Subsequently, the glass Petri dishes stored until further processing.

The assembly and disassembly of collectors, as well as sample handling, were performed by trained personnel belonging to the groups participating in the Spanish Network of Micro- and Nanoplastics in the Environment (www.enviroplanet.net). Throughout the sampling and processing stages, all plastic material was avoided and people in charge were instructed to wear cotton clothes. At each site and period, a third collector was employed as a procedural control. Procedural controls are the collector exposed to same experimental conditions as the two collectors except to capture bulk deposition. This includes that, during the assembly and disassembly stages at the beginning and end of the collection period, it was kept open. It was also used on occasions when maintenance operations were necessary during the experiments.

During manipulation in that laboratory, contamination controls were deployed, consisting of glass Petri dishes kept open during all procedures. There controls were analysed using the same methodology as the rest of the samples. Furthermore, during vacuum filtration, Milli-Q water was filtered 3 times through 1 µm filters to assess the contamination of water. In the controls, a total of 143 particles (16 fragments and 127 fibres) were found. Among them, 56 particles were identified as artificial non-plastic particles (ANPP) or plastic, while the remaining were natural particles (70) or particles that could not be unambiguously identified. Particles with the same typology and composition as those found in controls were removed from the corresponding samples. For example, in site 1 we found 1 blue cellulose fibre in the controls from Autumn sample, therefore we removed all blue cellulose fibres (1 blue cellulose fibre) from the list of artificial non-plastic particles in that sample. The details for all the particles found in controls and the actions taken are shown in Table S3 (SM).

3. Results and discussion

3.1. Characterization of atmospheric MP deposition

A total of 1189 particles with probable anthropogenic origin were individually recovered from the filters using metal tweezers or a needle. Among them, 445 randomly selected particles were analysed using micro-FTIR, which represented a maximum error of 3.7% calculated as explained elsewhere (Kedzierski et al., 2019). The total number of positively identified MPs was 223. Additionally, 69 particles were classified as ANPP because, despite they consisted of natural polymers, mostly cellulose, they presented non-natural colours or textures, indicating some kind of industrial processing. Industrially processed natural fibres may incorporate chemical additives including dyes, softeners, flame retardants, biocides, and antistatic agents, among others (Darbra et al., 2012). Many of these additives are synthetic compounds that can be released into the environment during use or after the discarded product is mismanaged. The rest of the particles were natural polymers (or natural macromolecules without sufficient evidence of industrial processing, which summed up to 98) and particles that could not be identified with sufficient evidence (55 particles).

The results revealed that the composition of MPs was dominated by fibres representing at least 70% of the MPs identified in all locations (average 74.8%). The rest were fragments, with very few films (<1%). The median size of MP fragments (equivalent diameter) was 67.7 μm (43.8, 95.7) and for fibres was 72.4 (57.8, 90.1). For fibres, the median length and width were 1014 μm (532, 1720) and 16 μm (13, 19). Interquartile ranges (25th and 75th percentiles) are those given in brackets. Fig. 2 shows the CFD function for the size distribution of all the MPs sampled in this work. The results indicate that the power law can be applied with scaling parameter of 4.10 ± 0.59 for sizes higher than $75.5 \pm 11.6 \mu\text{m}$ (fitted for all MPs, either fibres or fragments). The boundaries represent standard deviation obtained using bootstrapping with 1000 runs. Number-size distributions satisfying Eqs. (2 and 3) can be interpreted as a fractal distribution, where scaling parameter serves as the fractal fragmentation dimension, reflecting how fragmentation progresses from larger to smaller particles. In scenarios of mass conservation, it can be interpreted as evidence of a scale-invariant fragmentation mechanism. Consequently, the scaling parameter should approach 3 (remaining below that value) in 3D fragmentation as the probability of break-up increases. In the case of fibres, a one-

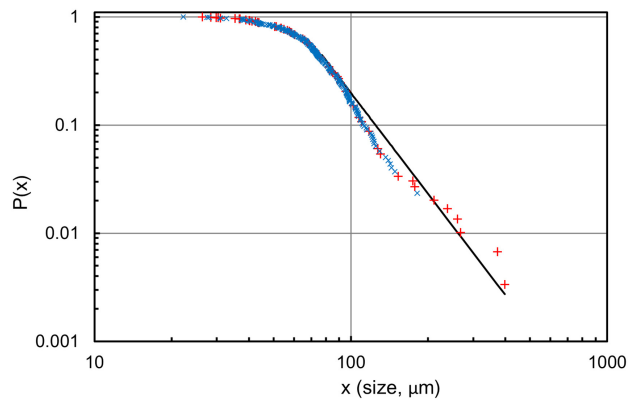


Figure 2: Particle size distributions as CFD, $P(\text{size} > x)$, of atmospheric MP deposition found in this work. Blue: fibres. Red: fragments and films.

dimensional fragmentation process would result in a lower scaling parameter because of the lower dimensionality of the fragmentation process (Kooi and Koelmans, 2019). However, environmental samples are not drawn from mass conservative systems. The fact that slope relating the number of fragments to their size in double logarithmic coordinates was > 3 can be interpreted as the consequence of a size selection mechanism that increases the share of smaller fragments in the samples. We hypothesize that this effect can be due to the higher mobility of small MPs, that would become overrepresented in atmospheric deposition samples.

Altogether, ten different polymers were found in the samples (Fig. 3), listed in order of abundance: polyester (PES), acrylic polymers (ACR), polypropylene (PP), polyurethane (PUR), alkyd resins (ALK), polyamide (PA), polyethylene (PE), polystyrene (PS), polyvinyl chloride (PVC) and polysulfone (PSU). The most abundant was by far PES, representing over 70% of the synthetic polymers identified, with the majority ($> 90\%$) in the form of fibres. Acrylic polymers, represented 10.5%, while PE, PS, PVC, and PSU displayed abundances $< 2\%$.

The higher abundance of synthetic fibres over fragments or films has been reported in other studies. Wright et al. found that 17% of the fibres recovered from the atmospheric fallout in Central London were synthetic, the most abundant of which was polyacrylonitrile (67%), followed by polyester/polyethylene terephthalate (PES/PET, 19%) and PA (9%). Other polymers found in lower amounts were PU, and PP. Additionally, a significant number of fibres (approximately 4% of the total fibre load) was identified as regenerated cellulose, an artificial fibre, while many other corresponded to cellulose, (69%) with probable anthropogenic origin (Wright et al., 2020). Roblin et al. studied the anthropogenic deposition of fibres in coastal areas of Ireland and found that the

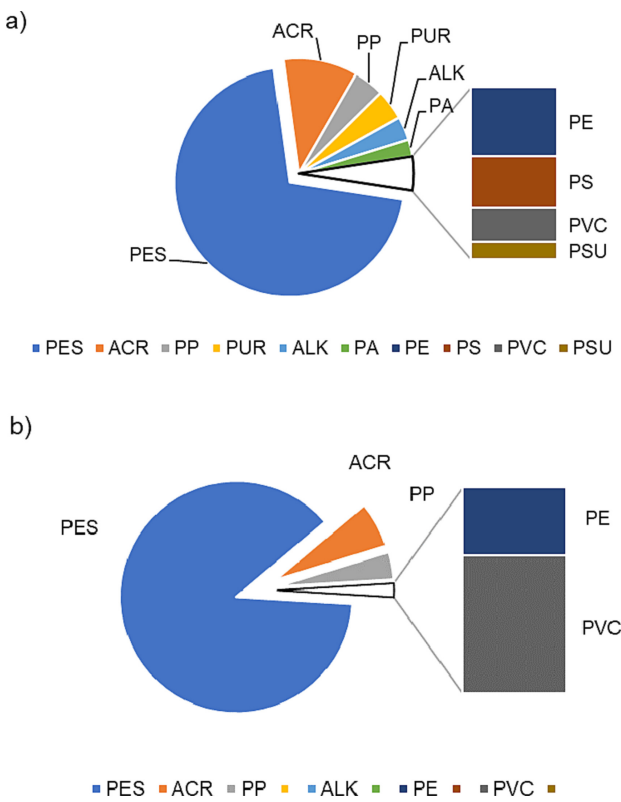


Figure 3: Chemical composition (percentages) of atmospheric MP deposition identified in this work. All types (a) and only fibres (b): Polyester (PES), acrylic polymers (ACR), polypropylene (PP), polyurethane (PUR), alkyd resins (ALK), polyamide (PA), polyethylene (PE), polystyrene (PS), polyvinyl chloride (PVC) and polysulfone (PSU).

higher abundance corresponded to polyester fibres (including PET, >70 % relative abundance) followed by polyacrylonitrile and PE (both >10 %) (Roblin et al., 2020). There is a relatively general agreement that PES is the main polymer among fibres in atmospheric studies (Beaurepaire et al., 2021).

3.2. Quantification of atmospheric MP deposition

The median of atmospheric MPs deposition rate in Spain ranged from 5.6 to 78.6 $\text{MPs m}^{-2} \text{ day}^{-1}$, with a median total MPs deposition rate of 15.1 $\text{MPs m}^{-2} \text{ day}^{-1}$ (with 25th and 75th percentiles at 7.0 and 38.8 $\text{MPs m}^{-2} \text{ day}^{-1}$, respectively), and maximum values slightly below 100 $\text{MPs m}^{-2} \text{ day}^{-1}$. This calculation was based on the proportion between positively identified particles and the particles recorded with the same colour and morphology in that specific location, taken from the whole set of particles with probable anthropogenic origin. Taken together, across all sites and sampling periods, the average coefficient of variation —defined as the ratio of the standard deviation to the mean— between the two collectors, was found to be 17 % (Fig. S2, SM). Deposition data

were calculated using the particles recovered from both collectors.

Comparing different locations, the most populated areas (Madrid in winter and Barcelona in spring) clearly showed higher median values of atmospheric MPs deposition than those with lower population densities (Tres Cantos and Alcalá de Henares in summer no plastic particles were detected). The statistical analysis indicated a significant positive correlation between the population of the study area (Table S1) and the median atmospheric MP deposition ($R^2 = 0.91$), suggesting that urban areas could act as sources of atmospheric MPs. However, average seasonal rates for the entire network were relatively similar, ranging from 22.3 $\text{MPs m}^{-2} \text{ day}^{-1}$ in summer to 29.6 $\text{MPs m}^{-2} \text{ day}^{-1}$ in autumn. The data are shown in Fig. 4a and detailed in Table S4 (SM). Tres Cantos and Alcalá de Henares are small and medium sized towns close to Madrid, but the stations were located in their outskirts, which may explain the lower values observed in the study (median values of 5.6 and 6.7 $\text{MPs m}^{-2} \text{ day}^{-1}$, respectively). Vigo, an industrial city in the northwest of Spain, also consistently displayed high deposition rates (median 44.1 $\text{MPs m}^{-2} \text{ day}^{-1}$), although lower than Madrid and Barcelona, likely due to the effect of marine winds. Apart from Madrid-Centre, the higher rates corresponded to the cities of Vigo, Barcelona, and Las Palmas de Gran Canaria. A significant negative correlation was found between the median wind speed (Table S2, SM) and the median of atmospheric MP deposition in all four seasons of the year ($R^2 = 0.89$) indicating that winds could clean the atmosphere from MPs, especially in coastal areas with winds bearing lower concentration of plastic particles. Furthermore, median rainfall showed a significant positive correlation with the median atmospheric MPs deposition in all four seasons of the year ($R^2 = 0.81$) suggesting that rainfall may also play a relevant role forcing the deposition of MPs (Table S1, SM).

Consistent with our results, urban areas had been previously associated to higher atmospheric fallout. (Table 1 presents a selection of results on atmospheric deposition rates of MPs taken from several recent studies.) Cai et al. (2017) studied the atmospheric fallout of MPs in the city of Dongguan (China, >8 million people) and found deposition rates in the 175 to 313 $\text{MPs m}^{-2} \text{ day}^{-1}$ range with fibres as the dominant shape. In Central London, Wright et al. (2020) found MPs fallout rates ranging from 575 to 1008 $\text{MPs m}^{-2} \text{ day}^{-1}$, essentially (>90 %) fibres. In a study performed in the megacity of São Paulo (>12 million inhab.) the average atmospheric fallout of MPs was $123.2 \pm 47.1 \text{ MPs m}^{-2} \text{ day}^{-1}$, with more fibres than fragments, especially PES fibres (Amato-Lourenço et

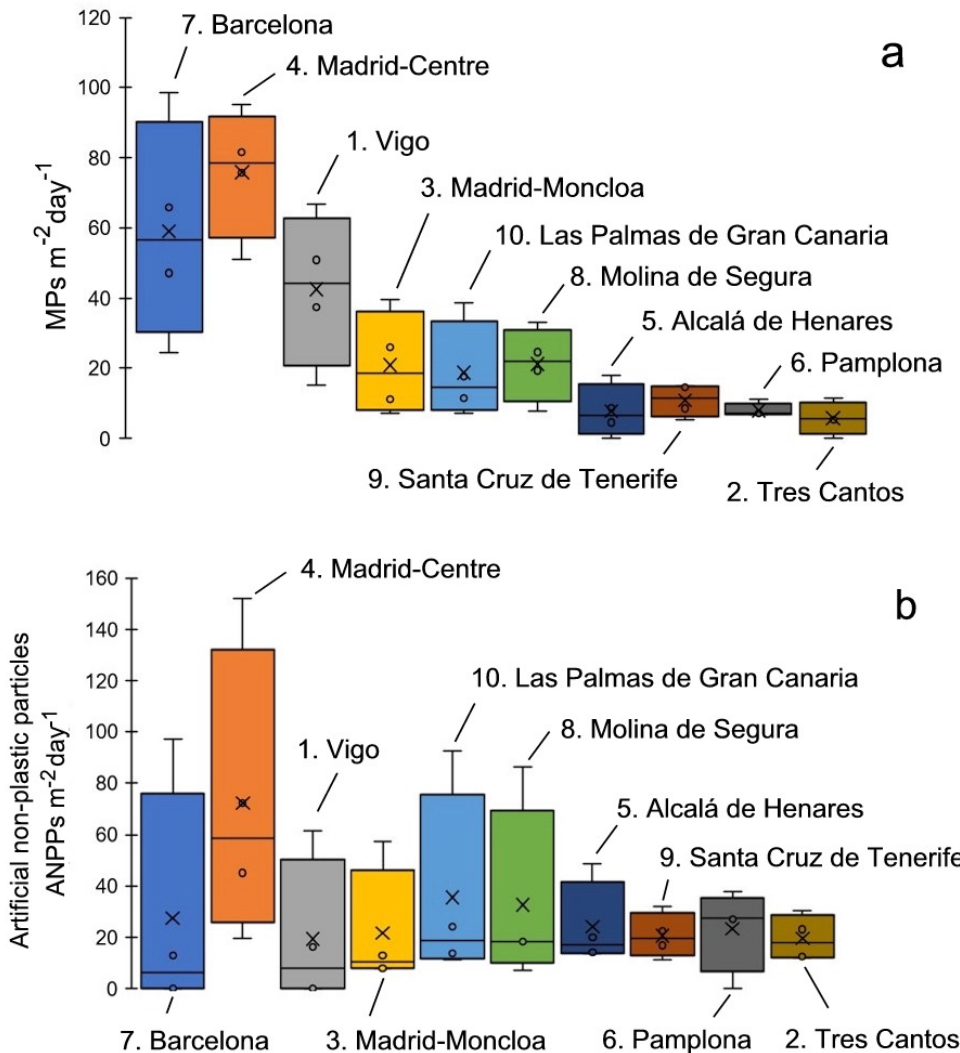


Figure 4: Deposition rates of MPs (a) and artificial non-plastic particles (b) as yearly median. The boxes represent the interquartile range and the bars the maximum and minimum seasonal values. Locations (numbers in brackets) in decreasing order of maximum deposition rates for MPs.

al., 2022). Consistent with the urban origin of most atmospheric MPs, suburban and less populated areas tended to display lower deposition rates. In coastal areas of Ireland, Roblin et al. (2020) found average deposition of MPs fibres of $12 \text{ MPs m}^{-2} \text{ day}^{-1}$. In a suburban site of New Zealand, the deposition rate recorded for plastics was in the $8\text{--}33 \text{ MPs m}^{-2} \text{ day}^{-1}$ range and mostly consisted of fibres (90 %) (Knobloch et al., 2021). However, the use of different size cutoffs and methodologies make comparisons challenging between these studies. In the most comprehensive study to date covering different areas with the same methodology, Brahney et al. (2020) reported the rates of MPs deposition in protected areas of the United States, finding that MP fibres comprised about two thirds of both wet and dry deposition with composition consistent with clothing textiles. In this study, deposition rate averaged $132 \text{ MPs m}^{-2} \text{ day}^{-1}$ and

their main source was attributed to urban centres. The authors used back-trajectory analyses to demonstrate that, in the absence of precipitations, smaller particles could travel long distances before reaching the ground. Mountain areas and remote regions have also registered high values for MPs deposition rate, which provides further evidence of their high mobility. Abbasi and Turner (2021) obtained deposition rates in a remote mountain site (Mount Derak) in Iran ranging from 7 to $180 \text{ MPs m}^{-2} \text{ day}^{-1}$.

Fig. 4b shows the deposition rate calculated for artificial non-plastic particles (ANPP), which were mostly (92.8 %) fibres. The median values for deposition rates ranged from 6.4 to $58.6 \text{ ANPPs m}^{-2} \text{ day}^{-1}$ range. The maximum values were obtained for Madrid and Barcelona with peaks of 152.1 and $97.0 \text{ ANPPs m}^{-2} \text{ day}^{-1}$, respectively, both occurring in winter. These particles mainly consisted of cellulosic

Table 1. Selection of recent data on the deposition rate of MPs.

Place	Site	Polymer type	Deposition rate (MPs m ⁻² day ⁻¹)	Reference
Paris, urban (site #1) and suburban (site #2)	Fibres predominant in the 200–400 µm and 400–600 µm ranges	Natural fibres (50 %), synthetic fibres (12 %), synthetic polymers (17 %)	110 ± 96 (mean, site #1) and 53 ± 38 (mean, site #2), overall 2–350 (range)	Dris et al. 2016
Dongguan city, China	Most fibres in the 200–700 µm range	Fibres were dominant (90.1 %); ~15 % were MPs	31 ± 8 to 43 ± 4 (range)	Cai et al. 2017
Pyrenees, remote area	Fibre lengths mostly in 100–300 µm range	Synthetic polymers	365 ± 69 (mean)	Allen et al. 2019
Hamburg, urban & periurban sites	Synthetic polymers (77 %); mostly (95 %)	275 (median), 137–512 (range)	Klein and Fischer 2019	
National Parks and Wild sites of the USA	Fibres between 20 µm and ~3 mm; fragments 4 and 188 µm	72.5% Synthetic fibres; 30 % of the rest were primary microbeads	132 ± 6 (mean), (48–435 range)	Brahney et al. 2020
Coastal areas of Ireland	Fibres mostly in the 200–600 µm size range	Anthropogenic and plastic fibres; 15 % of the fibres collected were plastic	12 (mean for plastic fibres)	Roblin et al. 2020
Central London	Modal diameter 20–25 µm (mean 24 ± 10 µm [SD]; most abundant lengths 400–500 µm (mean 905 ± 641 µm [SD]))	Fibres (92 %)	712 ± 162 (mean, fibres), 551–919 (range, fibres), 59 ± 32 (mean, fragments/granules), 12–99 (range, fragments/granules)	Wright et al. 2020
Two sites in Iran: Shiraz (urban) and Mount Derak	reaction < 100 µm predominant in all samples	Fibres (> 95 %)	64 (mean, Shiraz), 33–117 (range Shiraz), 12 (mean, Mount Derek), 7–18 (range, Mount Derak)	Abbasi and Turner 2021
Suburban site in Christchurch, New Zealand	Majority of fibres > 500 µm	Fibres (85.6 %)	123 ± 47 (mean)	Knobloch et al. 2021
São Paulo, Brazil (urban)	Most abundant fibre between 100 and 200 µm	Fibres (85.6 %)	123 ± 47 (mean)	Amato-Lourenço et al. 2022
Ten locations in Continental Spain and the Canary Islands	Median equivalent size for all particles 71 µm; fibres 1014 µm (median length) and 16 µm (median width); fragments 64 µm (median)	Fibres (74.8 %)	15.1 (median), 5.6–78.6 (range)	This work

fibres, primarily displaying red and blue colours, indicating evidence of having undergone industrial processing. The seasonal deposition rates are also shown in Table S5 (SM). Fibres, predominantly of textile origin, have been frequently detected in environmental samples, including the gastrointestinal tracts of vertebrates, and this has been attributed to the pollution by microscopic anthropogenic litter (Zhao et al., 2016). Although the environmental significance of natural textile fibres has received limited attention in the literature, their presence as anthropogenic pollutant has been firmly established. It has been argued that natural fibres should be included in environmental studies due to their potentially different role compared to synthetic fibres concerning degradation and interaction with chemicals (Ladewig et al., 2015). The case of artificial fibres, like industrially processed natural fibres, offers limited controversy. However, there are certain limitations in the spectroscopic characterization methods that make it difficult to differentiate natural fibres from industrially processed ones, including extruded textile fibres, unless they present specific colours (Stanton et al., 2019). Probably for this reason, the data on deposition rate of ANPPs displayed a higher variability than those of MPs, although they followed the same global trend (Table 1).

The detailed particle characterization performed in this work allowed an estimation of the total mass of plastic particles. To achieve this, the mass of each plastic particle was calculated using the diameter of the sphere with the same volume as the particle, d_V , and the density of the corresponding polymer. The total mass of particles was then divided by the deposition area, considering the whole set of collectors deployed, resulting an average value of $7.8 \text{ g km}^{-2} \text{ day}^{-1}$. This result is similar to the visual estimation performed by Brahney et al. (2021), who reported a range of $6.5\text{--}20.8 \text{ g km}^{-2} \text{ day}^{-1}$ for the deposition rate of plastic particles in protected areas of the United States (Brahney et al., 2021). Our data showed that densely populated cities may receive yearly $2\text{--}3 \times 10^4 \text{ MPs m}^{-2}$ ($2.1 \text{ and } 2.9 \times 10^4 \text{ MPs m}^{-2}$ are the median values for Barcelona and Madrid, respectively). For those cities, considering the surfaces of Madrid (604.3 km^2) and Barcelona (101.9 km^2). i.e.: the geographical area covered by their respective municipalities, the annual deposit of plastics would amount to 1.1 (Barcelona) and 9.0 (Madrid) tons of MPs. In contrast, the corresponding figures are much lower for the less populated locations, due to lower deposition rate and surface. For example, the estimated annual deposition for Tres Cantos would amount to only 40 kg. Furthermore, the case of Madrid revealed that samples taken in the outskirts of large cities (as in

the case of Madrid-Moncloa, station 3) may show significantly lower than those from city centres. In this case, Madrid-Moncloa, the sampling was performed near green areas populated by trees, which may act as a barrier to MPs resuspension.

4. Conclusions

This study presents the results of nationwide monitoring of atmospheric MPs deposition, providing comparable data from ten different urban areas sampled across four consecutive years' seasons. Our findings allowed us to determine the intrinsic variability of the method based on passive collectors and convert number rates into mass rates using geometric characterization of all individual particles. Besides MPs particles, our results allowed us to make the first estimation for the deposition of ANPP, which is another important component of atmospheric particulate pollution.

The yearly median of atmospheric deposition for all samples ranged from 5.6 to $78.6 \text{ MPs m}^{-2} \text{ day}^{-1}$, with a global median MPs deposition rate of $15.1 \text{ MPs m}^{-2} \text{ day}^{-1}$. The results showed that highly populated areas, such as Madrid-Centre and Barcelona, exhibited higher atmospheric MPs deposition values compared to less populated urban areas. The median value for ANPPs, mainly consisting of cellulose with non-natural colours and texture was $18.5 \text{ ANPPs m}^{-2} \text{ day}^{-1}$ (range $6.4\text{--}58.6 \text{ ANPPs m}^{-2} \text{ day}^{-1}$). The average MPs deposition in mass units was $7.8 \text{ g km}^{-2} \text{ day}^{-1}$ with a highest value of $50.9 \text{ g km}^{-2} \text{ day}^{-1}$.

The morphology of the MPs was clearly dominated by fibres, which represented almost three-quarters of the MPs identified in all locations, followed by fragments and films. Concerning the chemical composition, most of the MPs were polyester, representing over 70 % of the synthetic polymers identified, with the majority ($> 90 \%$) in the form of fibres. The rest consisted of acrylic and polypropylene fibres, as well as minor amounts of polyurethane, alkyd resins, and polyamide.

Acknowledgements

The authors acknowledge the support provided by Spanish Network of Plastics in the Environment, EnviroPlaNet (www.enviroplanet.net) and the financial support provided by the Spanish Government, Ministerio de Ciencia e Innovación, grants PID2020-113769RB-C21/C22. The authors would like to thank the Interdepartmental Investigation Research Service of the Universidad Autónoma de Madrid (SIDI-UAM and Segainvex) for the use of their infrastructures and their technical support. J.G.S. thanks ACIISI for

the contract from the Viera y Clavijo program at the University of La Laguna (85 % co-financed by the European Social Fund).

References

Abbasi, S., Turner, A., 2021. Dry and wet deposition of microplastics in a semi-arid region (shiraz, Iran). *Sci. Total Environ.* 786, 147358.

Allen, S., Allen, D., Phoenix, V.R., Le Roux, G., Durantez Jiménez, P., Simonneau, A., Binet, S., Galop, D., 2019. Atmospheric transport and deposition of microplastics in a remote mountain catchment. *Nat. Geosci.* 12, 339–344.

Amato-Lourenço, L.F., dos Santos, Galvão L., Wiebeck, H., Carvalho-Oliveira, R., Mauad, T., 2022. Atmospheric microplastic fallout in outdoor and indoor environments in São Paulo megacity. *Sci. Total Environ.* 821, 153450.

Batool, I., Qadir, A., Levermore, J.M., Kelly, F.J., 2022. Dynamics of airborne microplastics, appraisal and distributional behaviour in atmosphere; a review. *Sci. Total Environ.* 806, 150745.

Beaurepaire, M., Dris, R., Gasperi, J., Tassin, B., 2021. Microplastics in the atmospheric compartment: a comprehensive review on methods, results on their occurrence and determining factors. *Curr. Opin. Food Sci.* 41, 159–168.

Brahney, J., Hallerud, M., Heim, E., Hahnberger, M., Sukumaran, S., 2020. Plastic rain in protected areas of the United States. *Science* 368, 1257–1260.

Brahney, J., Mahowald, N., Prank, M., Cornwell, G., Klimont, Z., Matsui, H., Prather, K.A., 2021. Constraining the atmospheric limb of the plastic cycle. *Proc. Natl. Acad. Sci.* 118, e2020719118.

Cai, L., Wang, J., Peng, J., Tan, Z., Zhan, Z., Tan, X., Chen, Q., 2017. Characteristic of microplastics in the atmospheric fallout from Dongguan city, China: preliminary research and first evidence. *Environ. Sci. Pollut. Res.* 24, 24928–24935.

Darbra, R.M., Dan, J.R.G., Casal, J., Águeda, A., Capri, E., Fait, G., Schuhmacher, M., Nadal, M., Rovira, J., Grundmann, V., Barcelo, D., Ginebreda, A., Guillén, D., 2012. Additives in the textile industry. In: Bilitewski, B., Darbra, R.M., Barcelo, D. (Eds.), *Global Risk-Based Management of Chemical Additives I: Production. Usage and Environmental Occurrence*. Springer, Berlin Heidelberg, Berlin, Heidelberg, pp. 83–107.

dos Santos Galvão, L., Fernandes, E.M.S., Ferreira, R.R., dos Santos Rosa, D., Wiebeck, H., 2022. Critical steps for microplastics characterization from the atmosphere. *J. Hazard. Mater.* 424, 127668.

Dris, R., Gasperi, J., Saad, M., Mirande, C., Tassin, B., 2016. Synthetic fibers in atmospheric fallout: a source of microplastics in the environment? *Mar. Pollut. Bull.* 104, 290–293.

Evangelou, N., Grythe, H., Klimont, Z., Heyes, C., Eckhardt, S., Lopez-Aparicio, S., Stohl, A., 2020. Atmospheric transport is a major pathway of microplastics to remote regions. *Nat. commun.* 11 (1), 3381.

GESAMP, 2019. Guidelines on the monitoring and assessment of plastic litter and microplastics in the ocean. In: Kershaw P.J., Turra A. and Galgani F. (Eds.), *IMO/FAO/UNESCOIOC/UNIDO/WMO/IAEA/UN/UNEP/UNDP/ISA Joint Group of Experts on the Scientific Aspects of Marine Environmental Protection*, p. 130.

Gillespie, C.S., 2015. Fitting heavy tailed distributions: the poweRlaw package. *J. Stat. Softw.* 64, 1–16.

González-Pleiter, M., Edo, C., Aguilera, Á., Viúdez-Moreiras, D., Pulido-Reyes, G., González-Toril, E., Osuna, S., de Diego-Castilla, G., Leganés, F., Fernández-Piñás, F., Rosal, R., 2021. Occurrence and transport of microplastics sampled within and above the planetary boundary layer. *Sci. Total Environ.* 761, 143213.

Kedzierski, M., Villain, J., Falcou-Préfol, M., Kerros, M.E., Henry, M., Pedrotti, M.L., Bruzaud, S., 2019. Microplastics in Mediterranean Sea: a protocol to robustly assess contamination characteristics. *PloS One* 14, e0212088.

Klein, M., Fischer, E.K., 2019. Microplastic abundance in atmospheric deposition within the metropolitan area of Hamburg, Germany. *Science of The Total Environment* 685, 96–103.

Knobloch, E., Ruffell, H., Aves, A., Pantos, O., Gaw, S., Revell, L.E., 2021. Comparison of deposition sampling methods to collect airborne microplastics in Christchurch, New Zealand. *Water Air Soil Pollut.* 232, 133.

Kooi, M., Koelmans, A.A., 2019. Simplifying microplastic via continuous probability distributions for size, shape, and density. *Environ. Sci. Technol. Lett.* 6, 551–557.

Ladewig, S.M., Bao, S., Chow, A.T., 2015. Natural fibers: a missing link to chemical pollution dispersion in aquatic environments. *Environ. Sci. Technol.* 49, 12609–12610.

Liu, K., Wang, X., Wei, N., Song, Z., Li, D., 2019. Accurate quantification and transport estimation of suspended atmospheric microplastics in megacities: implications for human health. *Environ. Int.* 132, 105127.

NILU, 2020. Atmospheric Microplastic Collector. https://innovation.nilu.no/wp-content/uploads/sites/14/2020/04/innovation_nilu_Atmospheric_Microplastic_Collector_2020.pdf.

Österlund, H., Blecken, G., Lange, K., Marsalek, J., Gopinath, K., Viklander, M., 2023. Microplastics in urban catchments: Review of sources, pathways, and entry into stormwater. *Sci. Total Environ.* 858, 159781.

Pastorino, P., Pizzul, E., Bertoli, M., Anselmi, S., Kušće, M., Menconi, V., Pregro, M., Renzi, M., 2021. First insights into plastic and microplastic occurrence in biotic and abiotic compartments, and snow from a high-mountain lake (Carnic Alps). *Chemosphere* 265, 129121.

Plastics Europe, 2022. Plastics - The Facts 2022: An Analysis of European Plastics Production, Demand and Waste Data. PlasticsEurope. Association of Plastics Manufacturers, Brussels.

Roblin, B., Ryan, M., Vreugdenhil, A., Aherne, J., 2020. Ambient atmospheric deposition of anthropogenic microfibers and microplastics on the Western periphery of Europe (Ireland). *Environ. Sci. Technol.* 54, 11100–11108.

Rosal, R., 2021. Morphological description of microplastic particles for environmental fate studies. *Mar. Pollut. Bull.* 171, 112716.

Stanton, T., Johnson, M., Nathanail, P., MacNaughtan, W., Gomes, R.L., 2019. Freshwater and airborne textile fibre populations are dominated by 'natural', not microplastic, fibres. *Sci. Total Environ.* 666, 377–389.

Sun, J., Peng, Z., Zhu, Z.R., Fu, W., Dai, X., Ni, B.J., 2022. The atmospheric microplastics deposition contributes to microplastic pollution in urban waters. *Water Res.* 225, 119116.

Turcotte, D.L., 1986. Fractals and fragmentation. *J. Geophys. Res.* 91, 1921–1926.

Wang, T., Wang, L., Chen, Q., Kalogerakis, N., Ji, R., Ma, Y., 2020. Interactions between microplastics and organic pollutants: effects on toxicity, bioaccumulation, degradation, and transport. *Sci. Total Environ.* 748, 142427.

Wright, S.L., Ulke, J., Font, A., Chan, K.L.A., Kelly, F.J., 2020. Atmospheric microplastic deposition in an urban environment and an evaluation of transport. *Environ. Int.* 136, 105411.

Zhao, S., Zhu, L., Li, D., 2016. Microscopic anthropogenic litter in terrestrial birds from Shanghai, China: not only plastics but also natural fibers. *Sci. Total Environ.* 550, 1110–1115.

Supplementary Materials

A nationwide monitoring of atmospheric microplastic deposition

Carlos Edo¹, Francisca Fernández-Piñas^{2,3}, Francisco Leganes^{2,3}, May Gómez⁴, Ico Martínez⁴, Alicia Herrera⁴, Cintia Hernández-Sánchez⁵, Javier González-Sálamo⁵, Javier Hernández-Borges⁵, Joaquín López-Castellanos⁶, Javier Bayo⁶, Cristina Romera-Castillo⁷, David Elustondo⁸, Carolina Santamaría⁸, Rocío Alonso⁹, Héctor García-Gómez⁹, Rosario Gonzalez-Cascon¹⁰, Virtudes Martínez-Hernández¹¹, Junkal Landaburu-Aguirre¹¹, Mónica Incera¹², Jesús Gago¹², Beatriz Noya¹³, Ricardo Beiras¹³, Soledad Muniategui-Lorenzo¹⁴, Roberto Rosal^{1,*}, Miguel González-Pleiter^{2,3*}

¹Department of Chemical Engineering, Universidad de Alcalá, E-28871 Alcalá de Henares, Madrid, Spain

²Department of Biology, Faculty of Science, Universidad Autónoma de Madrid, E-28049 Madrid, Spain

³Centro de Investigación en Biodiversidad y Cambio Global (CIBC-UAM), Universidad Autónoma de Madrid, Madrid, Spain

⁴Ecophysiology of Marine Organisms (EOMAR), IU-ECOAQUA, Universidad de Las Palmas de Gran Canaria, Spain

⁵Applied Analytical Chemistry Research Group (AChem), Universidad de La Laguna, San Cristóbal de La Laguna, Spain

⁶Department of Chemical and Environmental Engineering, Technical University of Cartagena, Spain

⁷Instituto de Ciencias del Mar-CSIC, Barcelona, Spain

⁸Instituto de Biodiversidad y Medioambiente (BIOMA), Universidad de Navarra, Pamplona, Spain

⁹Centro de Investigaciones Energéticas, Medioambientales y Tecnológicas (CIEMAT), Madrid, Spain

¹⁰Department of Environment, National Institute for Agriculture and Food Research and Technology (INIA), Madrid, Spain

¹¹IMDEA-Water Institute, Alcalá de Henares, Madrid, Spain

¹²1 Instituto Español de Oceanografía (IEO-CSIC), Centro Oceanográfico de Vigo, Spain

¹³Centro de Investigación Marina de la Universidad de Vigo (CIM-UVigo), Spain

¹⁴University of Coruña, Grupo Química Analítica Aplicada (QANAP), Coruña, Spain

Contents:

Table S1. Population data and accumulated rainfall recorded from the State Meteorological Agency – Spanish Government (AEMET). The data correspond to the closest station to the sampling location.

Table S2. Maximum wind speed recorded in the closest station to the sampling location.

Table S3. Artificial non-plastic and plastic particles found in procedural controls. Polyester (PES), acrylic polymers (ACR), polypropylene (PP), polyurethane (PUR), alkyd resins (ALK), polyamide (PA), polyethylene (PE), polystyrene (PS), polyvinyl chloride (PVC) and polysulfone (PSU).

Table S4. Deposition rates of MPs per location and season.

Table S5. Deposition rates of artificial non-plastic particles (ANPP) per location and season.

Figure S1. Bespoke collector used and field set-up. (Photo taken in sampling point 3.)

Figure S2. Uncertainty estimation from duplicated collectors.

* Corresponding authors: roberto.rosal@uah.es, mig.gonzalez@uam.es

Table S1. Population data and accumulated rainfall recorded from the State Meteorological Agency – Spanish Government (AEMET). The data correspond to the closest station to the sampling location.

No.	Sampling location	Population (inhab.)	Rainfall (mm)				
			Annual mean	May-Jun 2021	Jun-Jul 2021	Nov-Dic 2021	Jan-Feb 2022
1	Vigo	293,642	1739	121.8	14.2	103.8	33.0
2	Tres Cantos	46,750	415	14.8	10.9	38.6	72.2
3,4	Madrid	3,200,000	415	25.6	1.4	14.4	1.5
5	Alcalá de Henares	193,751	489	12.5	0.8	16.8	3.0
6	Pamplona	362,390	784	96.2	26.4	530.4	27.8
7	Barcelona	1,620,000	614	5.2	1.2	52.2	0.8
8	Molina de Segura	70,964	272	94.6	0	60.0	4.0
9	Santa Cruz de Tenerife	204,856	281	25.8	11.8	163.6	126.4
10	Las Palmas de Gran Canaria	378,517	299	2.6	4.8	28.8	28.0
Accumulated, average							
				25.6	4.8	56.1	27.8

Table S2. Maximum wind speed recorded in the closest station to the sampling location.

No.	Sampling location	Maximum wind speed, average during the sampling period (km/h)			
		May-Jun 2021	Jun-Jul 2021	Nov-Dic 2021	Jan-Feb 2022
1	Vigo	24.6	22.9	26.5	20.8
2	Tres Cantos	28.8	28.5	26.9	27.1
3,4	Madrid	34.8	35.4	36.2	22.4
5	Alcalá de Henares	36.8	37.0	30.7	26.2
6	Pamplona	34.7	33.9	25.2	30.9
7	Barcelona	38.6	40.2	49.9	33.8
8	Molina de Segura	38.6	37.7	32.4	27.9
8	Santa Cruz de Tenerife	58.1	57.8	38.7	41.4
10	Las Palmas de Gran Canaria	35.7	34.8	25.2	30.9
Averages					
		35.3	35.1	30.4	27.5

Table S3. ANPPs and MPs found in procedural controls. Polyester (PES), acrylic polymers (ACR), polypropylene (PP), polyurethane (PUR), alkyd resins (ALK), polyamide (PA), polyethylene (PE), polystyrene (PS), polyvinyl chloride (PVC) and polysulfone (PSU).

Loc.	No.	Typology	micro-FTIR	Action taken in affected samples
1	1	White fragment	PE	No PE fragments in that sample
	1	Transparent fibre	PA	No PA fibres in that sample
	2	Yellow fibres	Cellulose	No yellow cellulose fibres in the affected samples
	2	Transparent fragments	PE	No PE fragments in the affected samples
	1	Red fibre	Cellulose	No red cellulose fibres in that sample
2	1	Blue fibre	Cellulose	1 blue cellulose fibre removed from the affected sample
	1	White fragment	PA	No PA fragments in that sample
	1	Yellow fibre	Cellulose	No yellow cellulose fibres in that sample
	1	Red fibre	ACR	No ACR fibres in that sample
	1	Transparent fibre	ACR	No ACR fibres in that sample
3	1	Transparent fibre	PES	No PES fibres in that sample
	1	White fragment	PA	No PA fragments in that sample
	2	Transparent fibres	PES	3 transparent PES fibres removed from two affected samples
	1	Blue fibre	Cellulose	1 blue cellulose fibre removed from the affected sample
	1	Yellow fibre	ACR	No ACR fibres in that sample
4	1	Black fibre	PES	1 black PES fibre removed from the affected sample
	2	Yellow fibres	Cellulose	No yellow cellulose fibres in the affected samples
	2	Transparent fibres	PES	5 PES transparent fibres removed from two samples
	1	Red fibre	Cellulose	No red cellulose fibres in that sample
	1	Blue fibre	Cellulose	1 blue cellulose fibre removed from the affected sample
5	2	Yellow fibres	Cellulose	No yellow cellulose fibres in the affected samples
	1	Red fibre	PES	1 red PES fibre removed from the affected sample
7	1	Red fibre	Cellulose	No red cellulose fibres in that sample
	1	Blue fibre	Cellulose	1 blue cellulose fibre removed from the affected sample
	1	Yellow fibre	Cellulose	No yellow cellulose fibres in that sample
	1	Transparent fibre	PP	No PP fibres in the affected sample
	1	Blue fibre	Cellulose	No blue cellulose fibres in that sample
8	1	Blue fragment	ALK	2 ALK fragment removed from the affected sample
	3	Yellow fibres	Cellulose	No yellow cellulose fibres in the affected samples
	2	Transparent fragment	PA	No PA fragments in the affected sample
	2	Blue fibres	Cellulose	2 blue cellulose fibres removed from the affected samples
	1	Red fibre	PA	No PA fibres in the affected sample
9	1	Black fibre	PA	No PA fibres in the affected sample
	1	Blue fibre	Cellulose	1 blue cellulose fibre removed from the affected sample
10	2	Yellow fibres	Cellulose	No yellow cellulose fibres in the affected samples
	1	Red fibre	Cellulose	1 red cellulose fibre removed from the affected sample
	1	Red fibre	Cellulose	No red cellulose fibres in the affected sample
	1	White fragment	PE	No PE fragments in the affected sample
	1	Transparent fragment	PP	No PP fragments in the affected sample
Lab.	1	Yellow fibre	Cellulose	No yellow cellulose fibres in the affected sample
	1	Blue fibre	Cellulose	No blue cellulose fibres in the affected sample
	2	Transparent fibres	PES	1 PES fibres removed from one affected sample
	2	Blue fibres	Cellulose	No blue cellulose fibres in the samples form that batch
Lab.	1	Yellow fibre	Cellulose	No yellow cellulose fibres in samples from that batch

Table S4. Deposition rates of MPs per location and season.

Loc.	Sampling point	MPs m ⁻² day ⁻¹			
		Spring	Summer	Autumn	Winter
1	Vigo	15.3	50.9	66.6	37.3
2	Tres Cantos	11.6	0	5.3	5.9
3	Madrid-Moncloa	11.0	7.0	39.5	26.0
4	Madrid-Centre	81.5	50.9	75.8	95.0
5	Alcalá de Henares	4.5	0	8.8	17.8
6	Pamplona	11.0	7.0	7.0	6.8
7	Barcelona	98.4	65.8	24.6	47.1
8	Molina de Segura	7.6	19.3	24.6	33.1
9	Santa Cruz de Tenerife	14.4	14.9	5.3	8.5
10	Las Palmas de Gran Canaria	11.5	7.0	38.6	17.5

Table S5. Deposition rates of ANPPs per location and season.

Loc.	Sampling point	ANPPs m ⁻² day ⁻¹			
		Spring	Summer	Autumn	Winter
1	Vigo	16.1	0	0	61.5
2	Tres Cantos	30.3	12.0	12.5	23.1
3	Madrid-Moncloa	7.8	8.0	11.8	57.4
4	Madrid-Centre	45.1	21.4	73.6	154.5
5	Alcalá de Henares	13.6	20.0	14.0	48.6
6	Pamplona	37.6	0	28.1	27.2
7	Barcelona	12.9	0	0	97.0
8	Molina de Segura	20.4	7.0	15.2	86.4
9	Santa Cruz de Tenerife	22.3	11.4	16.8	32.1
10	Las Palmas de Gran Canaria	13.6	24.2	11.1	89.5



Figure S1: Bespoke collector used and field set-up. (Photo taken in sampling point 3.)

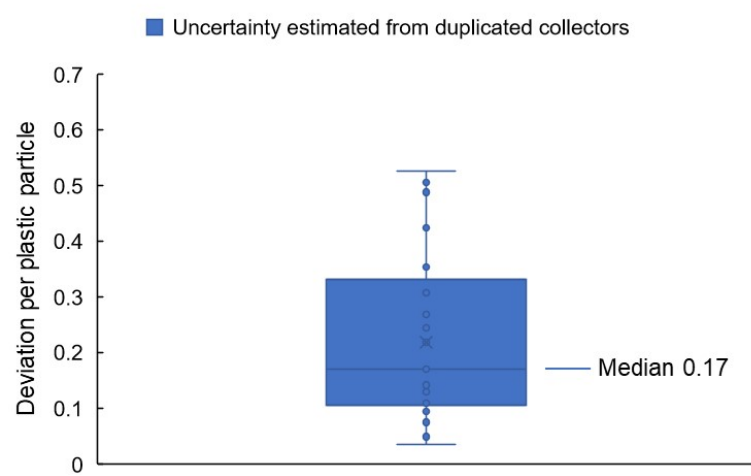


Figure S2: Uncertainty estimation from duplicated collectors.